Near-barrier fusion of $^{32}S + ^{90,96}Zr$: The effect of multi-neutron transfers in sub-barrier fusion reactions

H. Q. Zhang,[1] C. J. Lin,[1] F. Yang,[1] H. M. Jia,[1] X. X. Xu,[1] Z. D. Wu,[1] F. Jia,[1] S. T. Zhang,[1] Z. H. Liu,[1] A. Richard,[1,2,3] and C. Beck[2]

[1]*China Institute of Atomic Energy, P. O. Box 275(10), Beijing 102413, People's Republic of China*

[2]*Institut Pluridisciplinaire Hubert Curien, UMR 7178, CNRS-IN2P3, and Université de Strasbourg (UdS), F-67037 Strasbourg Cedex 2, France*

[3]*Ecole Nationale Supérieure de Physique de Strasbourg (ENSPS), F-67400 Illkirch, France*

(Received 13 April 2010; revised manuscript received 7 October 2010; published 15 November 2010)

Fusion excitation functions have been measured for the first time with rather good accuracy for $^{32}S + ^{90}Zr$ and $^{32}S + ^{96}Zr$ near and below the Coulomb barrier. The sub-barrier cross sections for $^{32}S + ^{96}Zr$ are much larger than for $^{32}S + ^{90}Zr$. A coupled-channels calculation considering the inelastic excitations is capable of describing sub-barrier enhancement only for $^{32}S + ^{90}Zr$. The unexplained part for $^{32}S + ^{96}Zr$ is found to be correlated with the positive-Q-value intermediate neutron transfers in this system. The comparison with $^{40}Ca + ^{96}Zr$ suggests that couplings to the positive-Q-value neutron transfer channels may play a role in the sub-barrier fusion enhancement. Multi-neutron transfers are taken into account in Zagrebaev's semiclassical model to explain the discrepancies of the sub-barrier fusion cross sections for $^{32}S + ^{96}Zr$.

DOI: 10.1103/PhysRevC.82.054609 PACS number(s): 25.70.Gh, 25.70.Jj, 24.10.Eq

I. INTRODUCTION

The heavy-ion fusion reactions in the low-energy range near and below the Coulomb barrier have been the subject of extensive experimental and theoretical efforts in the past decades [1–5]. In addition to the fact that the questions of the possible occurrence of unexpected phenomena, such as breakup effects on the fusion reactions at near-barrier energies [5,6], are still unresolved, one has also to understand better the role of neutron transfers in the fusion processes [7,8]. For instance, effects of neutron-rich projectiles on the formation of superheavy elements (SHEs) [9,10], especially with the development of newly available radioactive ion beam (RIB) facilities, need to be clarified, as well as fusion hindrance at extremely low energies, which remains among the most interesting open questions in the nuclear astrophysics domain [11–14]. Fusion enhancement below the Coulomb barrier is one of the most studied phenomena, and measurements of fusion barrier distributions have been widely performed to investigate the mutual importance of both the nuclear structure and dynamical process effects on the sub-barrier fusion enhancement [15–21].

Coupled-channels (CC) calculations have been used to describe the reactions in this energy range theoretically (see, for example, Refs. [3,15] and references therein). Fusion enhancement caused by the static deformations and surface vibrations of the nuclei has been well described in these coupled-channels calculations [15–21]. The influence of the neutron transfer channels on sub-barrier fusion processes [18–24] is not yet fully understood. During the last decades a large number of experimental and theoretical investigations have been undertaken to study the neutron transfer mechanisms in competition with the fusion processes. Stelson *et al.* [22–24] proposed an original scenario that used an empirical method involving a sequential transfer of several neutrons between the reactants. This multi-neutron transfer process is capable of initiating fusion at large internuclear distances and will smooth the fusion barrier distribution (with larger width) with a lower energy threshold. This "shift" effect corresponds to the energy window for which the nuclei are allowed to come sufficiently close together for neutrons to flow freely between the target and projectile. As a consequence, this will reduce the effective barrier and enhance the fusion cross sections at sub-barrier energies. Following this idea, Rowley *et al.* [25] used a simple phenomenological model that simulates couplings to neutron transfer channels with a parametrized coupling matrix. Later on, Zagrebaev [26] proposed another semiclassical theoretical model that has been successfully used to reproduce the sub-barrier fusion enhancement of the $^{40}Ca + ^{96}Zr$ reaction [18] by including the intermediate positive-Q-value neutron transfer channels in the CC calculations. Although damped by Coulomb repulsion, a similar effect might also be of importance for proton transfer, but very scarce results are available [2].

The failure of the CC calculations that include only the couplings to the inelastic excitations indicates that couplings to neutron transfer channels might play a key role in the fusion dynamics near the barrier for medium-heavy systems such as $^{40}Ca + ^{90,96}Zr$ [18,27], $^{28}Si + ^{90,94}Zr$ [28], and $^{20}Ne + ^{90,92}Zr$ [29], the last two reactions being studied by measurements of large-angle quasielastic scatterings. Our previous measurements of quasielastic scatterings of $^{32}S + ^{90,96}Zr$ were also undertaken at backward angles near the barrier [30]; the analysis gave an indication that positive-Q-value neutron transfer channels should be included in the coupling scheme. Up to now no fusion data exist for $^{20}Ne + ^{90,92}Zr$ or $^{32}S + ^{90,96}Zr$; it will be interesting to measure these fusion excitation functions. In order to disentangle the possible effect of positive-Q-value neutron transfer couplings, we decided to investigate the last two systems. We report here on the measurement of near- and sub-barrier fusion excitation functions of $^{32}S + ^{90,96}Zr$ performed with small energy steps and good statistical accuracy.

Our research will focus on the role of neutron transfers between the colliding nuclei as a mechanism to enhance the fusion cross sections at sub-barrier energies. This paper is organized as follows. Section II presents the experimental setup and details of the measurements. Results of the analysis of the experimental data are given in Sec. III. The discussion is finally presented in Sec. IV in the framework of comparisons with coupled-channels calculations, before a short summary in Sec. V.

II. EXPERIMENTAL PROCEDURES

The experiment was performed at the HI-13 tandem accelerator of the China Institute of Atomic Energy (CIAE), Beijing. A collimated ^{32}S ($q = 10+$ charge state) beam was used to bombard the zirconium oxide targets. The beam intensity was stabilized in the 2–20 pnA range in order to minimize the pile-up for each of the bombarding energies. The 3-mm-diameter (98.87% enriched) $^{90}ZrO_2$ and (86.4% enriched) $^{96}ZrO_2$ targets were both 50 μg/cm^2 thick and evaporated onto 15 μg/cm^2 carbon foil backings. The thicknesses of targets were estimated by using standard Rutherford backscattering measurements. The isotope correction for the 13.6% impurity in the ^{96}Zr targets was made as carefully as possible. A small isotope dependence of the fusion cross sections is known to occur mainly for energies above the Coulomb barrier. At energies well below the barrier, the fusion cross sections for $^{32}S + ^{90}Zr$ are very small and negligible compared with $^{32}S + ^{96}Zr$ cross sections. The most significant corrections were applied to the raw data. They ranged from 3% to 15% for energies below the Coulomb barrier. The corresponding errors have been estimated to be from 0.3% to 1.5%. These target thickness uncertainties are included in a total systematic error of approximately 15%. The beam energies were varied over the range $E_{lab} = 100$–130 MeV for $^{32}S + ^{90}Zr$ and $E_{lab} = 95$–130 MeV for $^{32}S + ^{96}Zr$ (in 1.33 MeV steps at the higher and 0.67 MeV at the lower energies) and changed only downward starting at $E_{lab} = 130$ MeV in order to reduce the magnetic hysteresis for both targets. Four silicon detectors placed symmetrically at $\theta = \pm 25^\circ$ (right-left and up-down) with respect to the beam direction were used to monitor the Rutherford scattering and to provide an absolute normalization of the fusion cross sections.

The fusion evaporation residues (ERs) concentrated within a few degrees of the incident beam direction were separated from the incident beam (see Fig. 1) by an electrostatic deflector [31]. It consists of two pairs of electrodes followed by an E vs time of flight (TOF) detector telescope with a microchannel plate (MCP) detector and a Si(Au) surface barrier detector. Two-dimensional plot of the data was used to cleanly separate the ERs from the beamlike products (BLPs). A typical example of the TOF versus energy spectrum for $^{32}S + ^{96}Zr$ measured at $E_{lab} = 130$ MeV and $\theta = 2^\circ$ is shown in Fig. 1. The distinction between ER events and other processes is straightforward at 2°, as shown by the two-dimensional spectrum of Fig. 1; such an easy analysis of ERs could be done similarly at larger angles (not shown in the figure). The electrostatic deflector could be rotated about the target position in the horizontal plane to measure the ER angular distribution.

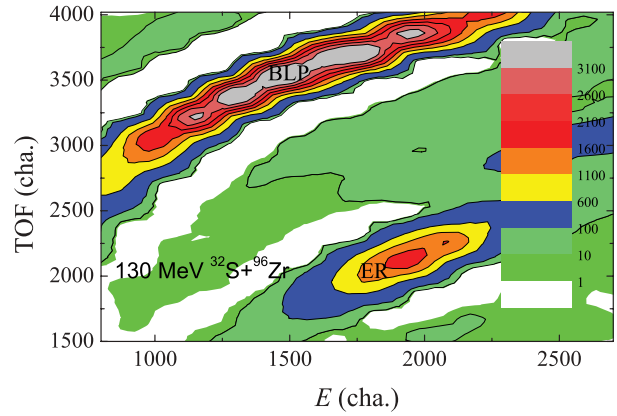

FIG. 1. (Color online) Two-dimensional plot E-TOF of the events following beam separation, taken at $E_{lab} = 130$ MeV and at 2° for the $^{32}S + ^{96}Zr$ reaction. Two groups of particles (ERs and BLPs) are indicated.

The particles from the target were selected before entering the fields by an entrance collimator of 3 mm diameter, corresponding to an opening angle $\Delta\theta = \pm 0.57^\circ$. A 10-$\mu$g/cm^2-thick carbon foil clinging to the collimator was used to reset the atomic charge state distribution on the ion path. The collimator of the MCP defined the solid angle of the electrostatic deflector as being approximately $\Delta\Omega = 0.3$ msr.

The ER angular distributions were measured in the range $\theta = -4^\circ$ to 10° with step $\Delta\theta = 1^\circ$ at three beam energies ($E_{lab} = 108.3$, 116.4, and 130.0 MeV) for both systems. The angular distributions for $^{32}S + ^{96}Zr$ are shown in Fig. 2. It is found that they are symmetrical about $\theta = 0^\circ$, as expected. Their typical shapes do not change appreciably with the beam energy. These combined angular distributions and double Gaussian fits were used to obtain the fusion cross sections. At each energy the number of ER events was normalized to the Rutherford scattering rates counted by the monitor detectors. For most of the energy points, only differential cross sections were measured at $\theta = 2^\circ$; from the values obtained, the total

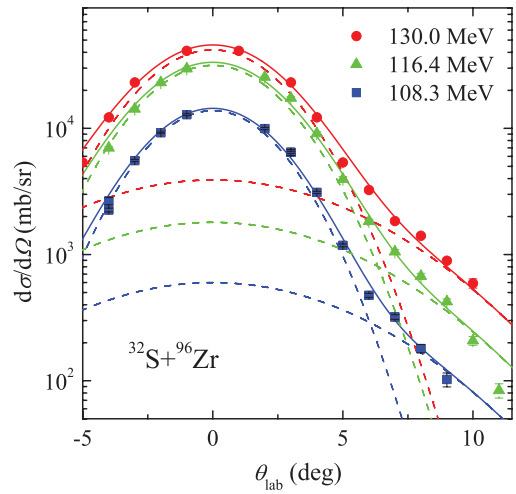

FIG. 2. (Color online) The angular distributions of fusion evaporation residues of $^{32}S + ^{96}Zr$ at three beam energies. The dashed lines are the two Gaussian functions used to obtain the total cross sections.

ER cross sections were deduced. Using the solid angles, the ($\theta = 2^\circ$)-to-total ratios, and the measured transmission efficiencies, these ER yields were transformed into total cross sections. The reproducibility of the measurement was checked during the experiment; for example, the two measurement results at -3° in the angular distribution at 108.3 MeV are coincident within the errors. Since fission of the compound nucleus can be neglected for both systems, the measured cross sections were taken as complete fusion cross sections σ_F.

The transmission efficiencies and the relevant voltages used to deflect the ERs were calibrated with a ^{122}Ba beam scattered by the ^{90}Zr target at small angles and at the corresponding energies to the ERs. It was found that the defocusing effect of the deflection voltage reduces the transmission from unity to 0.60 ± 0.06. Additional systematic errors come from the geometrical solid angle uncertainties, the angular distribution integrations, isotope correction errors, and the transmission measurements. Altogether these contributions sum up to a 15% value for systematic errors.

III. EXPERIMENTAL RESULTS

The fusion excitation functions first measured for the two systems are shown in Fig. 3, where the energy scale is corrected for the target thickness. The statistical errors shown in the figure do not exceed the symbol size for most of the experimental points. They are $\pm 0.8\%$ for both the high-energy and the intermediate-energy points and increase to $\pm 23\%$ for the low-energy points. The fusion cross sections are listed in Tables I and II for both reactions.

The comparison of the renormalized fusion functions [6] of $^{32}S + ^{96}Zr$ (present work) and $^{40}Ca + ^{96}Zr$ [18] is shown in Fig. 4. According to Canto *et al.* [6,32]

$$\bar{F}_{\rm expt}(x) = F_{\rm expt}(x)\frac{\sigma_F^W}{\sigma_{\rm CC}} \quad \text{with} \quad x = \frac{E_{\rm c.m.} - V_B}{\hbar\omega}, \tag{1}$$

$$F_{\rm expt}(x) = \frac{2E_{\rm c.m.}}{\hbar\omega R_B^2}\sigma_F^{\rm expt}, \tag{2}$$

TABLE I. Experimental fusion cross sections for $^{32}S + ^{90}Zr$.

$E_{\rm c.m.}$ (MeV)	$\sigma_{\rm F}$ (mb)	$E_{\rm c.m.}$ (MeV)	$\sigma_{\rm F}$ (mb)
95.3	623.51 ± 4.00	82.7	142.10 ± 1.37
94.2	582.98 ± 4.63	82.2	122.84 ± 1.08
93.3	528.80 ± 3.93	81.7	105.94 ± 1.10
92.2	535.48 ± 4.70	81.2	91.59 ± 0.92
91.2	430.00 ± 3.37	80.7	77.96 ± 0.80
90.7	442.29 ± 3.03	80.2	63.69 ± 0.62
90.2	429.44 ± 3.58	79.7	54.96 ± 0.55
89.7	363.05 ± 3.22	79.2	40.22 ± 0.39
89.2	357.17 ± 2.84	78.7	32.89 ± 0.34
88.7	342.70 ± 2.94	78.2	23.41 ± 0.35
88.2	322.27 ± 3.07	77.7	17.46 ± 0.35
87.7	309.41 ± 2.80	77.2	10.58 ± 0.42
87.2	298.07 ± 2.85	76.7	5.89 ± 0.41
86.7	277.99 ± 2.29	76.2	3.66 ± 0.37
86.2	246.27 ± 2.81	75.7	2.07 ± 0.25
85.7	244.09 ± 2.02	75.2	1.09 ± 0.16
85.2	224.93 ± 1.95	74.7	0.57 ± 0.10
84.7	190.06 ± 1.64	74.2	0.31 ± 0.06
84.2	189.70 ± 1.75	73.7	0.18 ± 0.04
83.7	167.85 ± 1.25	73.2	0.12 ± 0.03
83.2	143.85 ± 1.38		

and

$$\mathrm{UFF} = \ln[1 + \exp(2\pi x)], \tag{3}$$

where V_B, R_B, and $\hbar\omega$ are the fusion barrier height, radius, and curvature, respectively. σ_F^W and $\sigma_{\rm CC}$ are the fusion cross sections in the single-channel case approximated by the Wong model [33] and from the CC calculations including all relevant couplings to bound channels without neutron transfers. This comparison demonstrates the essential importance of transfer couplings in both reactions. One observes that the two systems display very similar behaviors over the whole energy range. The difference between the experimental results and the UFF below the barrier energies means that the channel couplings

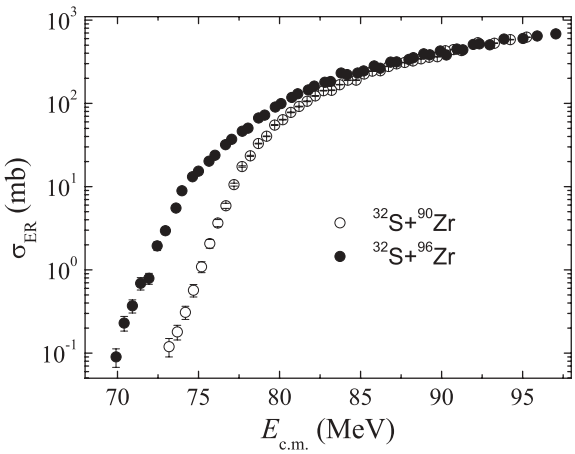

FIG. 3. Experimental fusion excitation functions of $^{32}S + ^{90}Zr$ (open circles) and $^{32}S + ^{96}Zr$ (solid circles) as a function of the center-of-mass energy. The error bars represent purely statistical uncertainties.

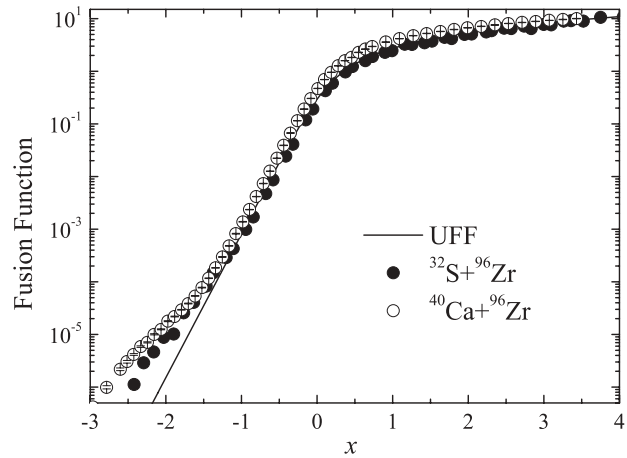

FIG. 4. Dimensionless fusion functions $\bar{F}_{\rm expt}(x)$ for $^{32}S + ^{96}Zr$ (filled circles) measured in the present work and $^{40}Ca + ^{96}Zr$ (open circles). UFF is the universal fusion function as obtained by Canto *et al.* [6,32]. The data for $^{40}Ca + ^{96}Zr$ are taken from Ref. [18].

TABLE II. Experimental fusion cross sections for $^{32}S + ^{96}Zr$.

$E_{c.m.}$ (MeV)	σ_F (mb)	$E_{c.m.}$ (MeV)	σ_F (mb)
97.1	683.96 ± 3.93	82.1	161.35 ± 1.34
95.9	644.56 ± 7.76	81.8	145.06 ± 1.51
95.0	601.59 ± 3.70	81.1	130.62 ± 1.09
93.9	591.22 ± 4.33	80.8	117.57 ± 1.21
93.0	505.50 ± 3.00	80.1	99.28 ± 0.85
92.3	519.80 ± 4.10	79.7	90.53 ± 0.83
92.0	510.25 ± 3.57	79.1	72.13 ± 0.66
91.3	439.19 ± 3.38	78.7	66.85 ± 0.70
90.9	448.78 ± 3.14	78.1	50.41 ± 0.43
90.3	381.53 ± 2.95	77.7	46.28 ± 0.51
89.9	424.93 ± 3.13	77.0	37.01 ± 0.31
89.3	382.96 ± 3.02	76.7	31.81 ± 0.34
88.9	393.91 ± 2.55	76.0	23.82 ± 0.03
88.3	354.74 ± 2.11	75.7	20.18 ± 0.03
88.0	338.00 ± 2.74	75.0	15.32 ± 0.23
87.2	314.40 ± 2.44	74.6	13.12 ± 0.26
86.9	313.05 ± 2.37	74.0	8.95 ± 0.36
86.2	264.38 ± 2.37	73.6	5.53 ± 0.39
85.8	282.11 ± 2.51	73.0	2.95 ± 0.30
85.2	244.76 ± 1.78	72.5	1.94 ± 0.23
84.8	231.95 ± 2.18	71.9	0.79 ± 0.12
84.2	222.32 ± 1.83	71.4	0.69 ± 0.12
83.8	231.63 ± 1.93	70.9	0.37 ± 0.07
83.2	182.87 ± 1.85	70.4	0.23 ± 0.05
82.8	179.30 ± 1.82	69.9	0.09 ± 0.02

are very important in both reactions. Further this comparison measures the importance of transfer couplings [34,35]. This behavior, already discussed in our previous investigation of $^{32}S + ^{90,96}Zr$ quasielastic barrier distributions [30], indicates that the positive-Q-value neutron transfers strongly enhance the fusion cross sections at sub-barrier energies. The present experimental observation is confirmed by the CC calculations in Zagrebaev's semiclassical model as discussed in the following section.

IV. COUPLED-CHANNELS CALCULATIONS

The fusion excitation functions of $^{32}S + ^{90,96}Zr$ have been calculated by means of the coupled-channels theory with the CCDEF code [36]. The potential barriers were found to be at $V_B = 81.2$ MeV, $R_B = 10.59$ fm, and $\hbar\omega = 3.98$ MeV for $^{32}S + ^{90}Zr$, and $V_B = 79.3$ MeV, $R_B = 10.86$ fm, and $\hbar\omega = 3.88$ MeV for $^{32}S + ^{96}Zr$. The related information on the low-lying excitations of ^{32}S, ^{90}Zr, and ^{96}Zr can be seen in Table III. The deformation parameters β_λ are taken from Refs. [37,38]. The quadrupole vibrations of both ^{90}Zr and ^{96}Zr nuclei are weak in energy; in fact, they lie at comparable energies.

Figure 5 shows the comparison of the experimental fusion excitation functions and the uncoupled and CC calculations without neutron transfers for the $^{32}S + ^{90}Zr$ fusion reaction. The CC calculation (solid line), which reproduces the data above and below the barrier V_B (arrow in Fig. 5), is quite satisfactory.

TABLE III. Excitation energies E_x, spin and parities λ^π, and deformation parameters β_λ for ^{32}S and $^{90,96}Zr$. The data are from Refs. [37,38]

Nucleus	E_x (MeV)	λ^π	β_λ
^{32}S	2.230	2^+	0.32
	5.006	3^-	0.40
^{90}Zr	2.186	2^+	0.09
	2.748	3^-	0.22
^{96}Zr	1.751	2^+	0.08
	1.897	3^-	0.27

Figure 6 shows the comparison of the experimental fusion excitation functions and the uncoupledand CC calculations without neutron transfers for the $^{32}S + ^{96}Zr$ fusion reaction. The CC calculation without neutron transfers fails for $^{32}S + ^{96}Zr$, with large discrepancies occurring mainly at energies below the barrier V_B (arrow in Fig. 6). A similar conclusion has been obtained for $^{40}Ca + ^{94}Zr$ [21]. It can be seen from Fig. 5 that the CC calculation reproduces the experimental excitation function well without considering neutron transfers for $^{32}S + ^{90}Zr$, while it fails for $^{32}S + ^{96}Zr$. The result shows that the enhancement of the sub-barrier fusion cross sections might be caused by multi-neutron transfers with positive Q values.

To take into account the neutron transfers, the fusion excitation function can be derived by using the following formula according to Zagrebaev's semiclassical model [26]:

$$T_l(E_{c.m.}) = \int f(B)\frac{1}{N_{tr}}\sum_k \int_{-E_{c.m.}}^{Q_0(k)} \alpha_k(E_{c.m.}, l, Q) \times P_{HW}(B, E_{c.m.} + Q, l) dQ dB \quad (4)$$

and

$$\sigma_F(E_{c.m.}) = \frac{\pi\hbar^2}{2\mu E_{c.m.}}\sum_{l=0}^{l_{cr}}(2l+1)T_l(E_{c.m.}), \quad (5)$$

where $T_l(E_{c.m.})$ is the penetration probability, B and $f(B)$ are the barrier height and the normalized barrier distribution function,

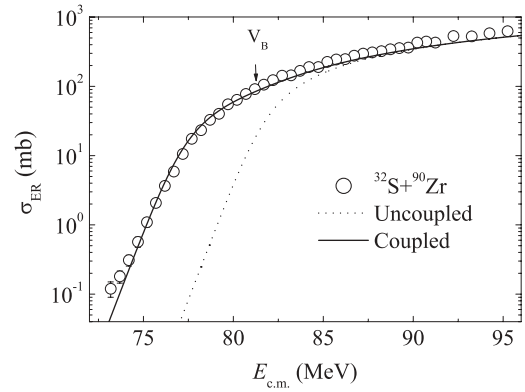

FIG. 5. Fusion excitation function of $^{32}S + ^{90}Zr$. The open circles are the experimental data. The dotted and solid lines represent the uncoupled and the CC calculations without neutron transfers. The arrow indicates the position of the Coulomb barrier for $^{32}S + ^{90}Zr$.

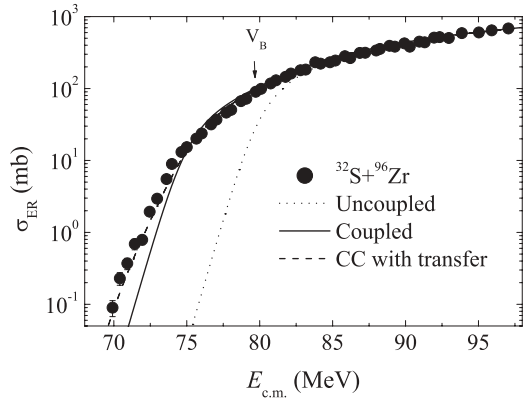

FIG. 6. Fusion excitation function of $^{32}S + ^{96}Zr$. The solid circles are the experimental data. The dotted, solid, and dashed lines are the uncoupled calculation and CC calculations without and with neutron transfers, respectively. The arrow indicates the position of the Coulomb barrier for $^{32}S + ^{96}Zr$.

which are taken from the CCDEF code, P_{HM} is the usual Hill-Wheeler formula [39], l is the momentum, and l_{cr} is the critical angular momentum. $\alpha_k(E_{c.m.},l,Q)$ is the probability for the transfer of k neutrons with $Q \leqslant Q_0(k)$, $Q_0(k)$ is the Q value for the ground-state to ground-state transfer of the kth neutron, and N_{tr} is the normalization of the total probability taking into account the multi-neutron transfers.

The calculation with the neutron transfer effect is performed up to the channel $+4n$ ($k = 4$). No more visible effect can be obtained by using $+5n$ and $+6n$ channels. The Q values for the calculation (dashed line in Fig. 6) are given in Table IV. As we can see in Fig. 6, the solid line (without neutron transfers) does not at all describe the data at sub-barrier energies. In contrast, the dashed line taking into account neutron transfers is able to reproduce the data reasonably well. As expected, the correction applied to the calculation at sub-barrier energies by the Zagrebaev model [26,40] enhances the cross sections further. Moreover, it allows a fairly good description of the present experimental data showing the effect of neutron transfers for the sub-barrier fusion of $^{32}S + ^{96}Zr$.

Figure 7 shows the experimental barrier distributions from fusion and quasielastic scattering and the corresponding calculations for both systems. The fusion barrier distributions for both systems have been obtained by double differentiation of $E\sigma_F$ versus energy using the three-point difference formula [18]. The quasielastic barrier distributions are taken from Ref. [30]. It is very interesting to note that for both reactions the experimental quasielastic barrier distributions and the experimental fusion barrier distributions are strikingly similar. Although a fine structure appears visible in the experimental fusion barrier distribution of $^{32}S + ^{96}Zr$, its damping is most

TABLE IV. Q-value in MeV for neutron pickup transfer channels from ground state to ground state for $^{32}S + ^{90,96}Zr$.

System	+1n	+2n	+3n	+4n
$^{32}S + ^{90}Zr$	−3.33	−1.229	−6.59)	−6.319
$^{32}S + ^{96}Zr$	0.788	5.737	4.508	7.655

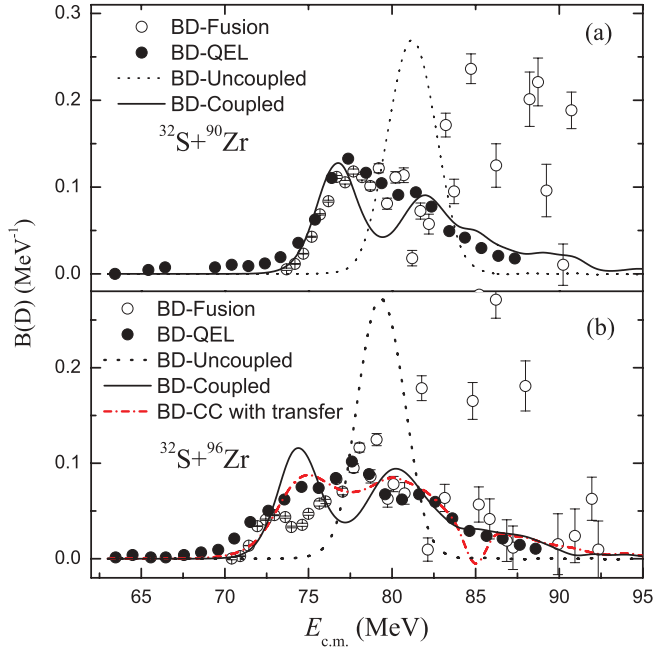

FIG. 7. (Color online) Barrier distributions from fusion (open circles) and quasielastic scattering (solid circles) for $^{32}S + ^{90}Zr$ (a) and $^{32}S + ^{96}Zr$ (b). The dotted, solid, and dash-dotted lines represent the uncoupled calculations and the CC calculations without and with neutron transfers, respectively.

probably caused by the strong octupole vibration in ^{96}Zr [21]. The actual discrepancies between calculated and experimental results are not yet fully understood. Large fluctuations occur in the fusion barrier distributions for $E_{c.m.} > 83$ MeV owing to the large errors of the ER cross sections in the high energy range. For $^{32}S + ^{90}Zr$, the overall trends of the experimental barrier distributions are roughly consistent with the CC calculation, while for $^{32}S + ^{96}Zr$, the experimental barrier distributions are wider and trend to a lower energy range compared with the results for $^{32}S + ^{90}Zr$ and the CC calculation without considering neutron transfers. This shows the effect of the $Q > 0$ neutron transfers on the sub-barrier fusion enhancement. The situation is very similar to $^{40}Ca + ^{96}Zr$ [18] whose fusion function behavior has been well illustrated in Fig. 4 by its comparison to the UFF [6].

For both projectiles ^{40}Ca and ^{32}S, we observe a significant widening of the fusion barrier distributions when neutrons are picked up from the ^{96}Zr target. This behavior is similar to what was concluded from the quasielastic barrier distributions of the two systems $^{32}S,^{40}Ca + ^{96}Zr$: they are wider and flatter than those for $^{32}S,^{40}Ca + ^{90}Zr$. This might partly justify the model of Stelson and co-workers [22–24] that neutron transfer channels could act as a doorway toward fusion [41,42]. Although damped by Coulomb repulsion, similar effects might also be of importance for proton transfer channels but very scarce results are available in the literature. Therefore, to reach a more general understanding of the role of nucleon transfers (i.e., both neutron and proton transfers) in the fusion processes below the Coulomb barrier, we will need more high-precision experimental fusion data with higher statistics at very low

incident energies. At the same time, the Zagrebaev model including the multiproton transfer should be extended.

V. SUMMARY

The fusion excitation functions for $^{32}S + ^{90,96}Zr$ were first measured with rather good accuracy near and below the Coulomb barrier. The sub-barrier cross sections for $^{32}S + ^{96}Zr$ are much larger than those for $^{32}S + ^{90}Zr$. The data have been analyzed in the framework of a coupled-channels approach. Good agreement between experimental data and the calculation is achieved for $^{32}S + ^{90}Zr$ by including the couplings to the low-lying quadruple and octupole vibrations in ^{32}S and ^{90}Zr. The calculation can reproduce the $^{32}S + ^{96}Zr$ data only by including four sequential neutron transfer channels as well as the low-lying quadrupole and octupole vibrations in ^{32}S and ^{96}Zr in Zagrebaev's semiclassical model. The result supports the previous suggestion [30] that positive-Q-value neutron transfer channels enhance sub-barrier fusion cross sections, particularly at very low energies. Also the fusion and quasielastic barrier distributions of $^{32}S + ^{90,96}Zr$ are essentially consistent in both cases. For $^{32}S + ^{96}Zr$, the experimental barrier distributions are wider and trend to a lower-energy range compared with $^{32}S + ^{90}Zr$ and the CC calculation without neutron transfers. This fact shows again the effect of the $Q > 0$ neutron transfers on the sub-barrier fusion processes. In addition to the fusion excitation function, the neutron transfer cross section measurement for this system should provide useful information on the coupling strength of neutron transfer channels, which will allow us to reach a much deeper understanding of the role of neutron transfer mechanisms, sequential or simultaneous, in the fusion processes.

ACKNOWLEDGMENTS

This work was supported by the National Natural Science Foundation of China under Grants No. 10575134, No. 10675169, and No. 10735100, and the Major State Basic Research Developing Program under Grant No. 2007CB815003, as well as the Boussole Grant No. 080105519 from Region Alsace (France) received by A.R. Two of us (A.R. and C.B.) would like to thank all the members of the experimental team of CIAE Beijing for their very kind hospitality and assistance.

[1] R. Pengo, D. Evers, K. E. G. Löbner, U. Quade, K. Rudolph, S. J. Skorka, and I. Weidl, Nucl. Phys. A **411**, 255 (1983).
[2] S. J. Skorka, A. M. Stefanini, G. Fortuna, R. Pengo, W. Meczynski, G. Montagnoli, A. Tivelli, S. Beghini, C. Signorini, and P. R. Pascholati, Z. Phys. A **328**, 355 (1987).
[3] A. B. Balantekin and N. Takigawa, Rev. Mod. Phys. **70**, 77 (1998).
[4] M. Dasgupta, D. J. Hinde, N. Rowley, and A. M. Stefanini, Annu. Rev. Nucl. Part. Sci. **48**, 401 (1998).
[5] L. F. Canto, P. R. S. Gomes, R. Donangelo, and M. S. Hussein, Phys. Rep. **424**, 1 (2006).
[6] L. F. Canto, R. R. S. Gomes, J. Lubian, L. C. Chamon, and E. Crema, J. Phys. G **36**, 015109 (2009)
[7] R. A. Broglia, C. H. Dasso, S. Landowne, and A. Winther, Phys. Rev. C **27**, 2433 (1983).
[8] S. Y. Lee, Phys. Rev. C **29**, 1932 (1984).
[9] V. I. Zagrebaev, V. V. Samarin, and W. Greiner, Phys. Rev. C **75**, 035809 (2007).
[10] W. Loveland, Phys. Rev. C **76**, 014612 (2007).
[11] M. S. Smith and K. E. Rehm, Annu. Rev. Nucl. Part. Sci. **51**, 91 (2001).
[12] C. L. Jiang *et al.*, Phys. Rev. Lett. **89**, 052701 (2002).
[13] C. L. Jiang, K. E. Rehm, B. B. Back, and R. V. F. Janssens, Phys. Rev. C **75**, 015803 (2007).
[14] C. L. Jiang, K. E. Rehm, B. B. Back, and R. V. F. Janssens, Phys. Rev. C **79**, 044601 (2009).
[15] N. Rowley, G. R. Stachler, and P. H. Stelson, Phys. Lett. B **254**, 25 (1991).
[16] J. X. Wei, J. R. Leigh, D. J. Hinde, J. O. Newton, R. C. Lemmon, S. Elfstrom, J. X. Chen, and N. Rowley, Phys. Rev. Lett. **67**, 3368 (1991).
[17] A. M. Stefanini *et al.*, Phys. Rev. Lett. **74**, 864 (1995).
[18] H. Timmers, D. Ackermann, S. Beghini, L. Corradi, J. H. He, G. Montagnoli, F. Scarlassara, A. M. Stefanini, and N. Rowley, Nucl. Phys. A **633**, 421 (1998).
[19] M. Trotta, A. M. Stefanini, L. Corradi, A. Gadea, F. Scarlassara, S. Beghini, and G. Montagnoli, Phys. Rev. C **65**, 011601(R) (2001).
[20] A. M. Stefanini *et al.*, Phys. Rev. C **73**, 034606 (2006).
[21] A. M. Stefanini *et al.*, Phys. Rev. C **76**, 014610 (2007).
[22] P. H. Stelson, Phys. Lett. B **205**, 190 (1988).
[23] P. H. Stelson, H. J. Kim, M. Beckerman, D. Shapira, and R. L. Robinson, Phys. Rev. C **41**, 1584 (1990).
[24] D. Shapira, and P. H. Stelson, Phys. Rev. C **47**, 1666 (1993).
[25] N. Rowley, I. J. Thompson, and M. A. Nagarajan, Phys. Lett. B **282**, 276 (1992).
[26] V. I. Zagrebaev, Phys. Rev. C **67**, 061601(R) (2003).
[27] G. Montagnoli, S. Beghini, F. Scalassara, A. M. Stefanini, L. Corradi, C. J. Lin, G. Pollarolo, and Aage Winther, Eur. Phys. G. A **15**, 351 (2002).
[28] Sunil Kalkal *et al.*, Phys. Rev. C **81**, 044610 (2010).
[29] E. Piasecki *et al.*, Phys. Rev. C **80**, 054613 (2009).
[30] F. Yang, C. J. Lin, X. K. Wu, H. Q. Zhang, C. L. Zhang, P. Zhou, and Z. H. Liu, Phys. Rev. C **77**, 014601 (2008).
[31] H. Q. Zhang, C. J. Lin, F. Yang, H. M. Jia, P. Zhou, G. P. An, C. L. Zhang, and X. X. Xu, Chin. Phys. C **34**, 1628 (2010).
[32] L. F. Canto, P. R. S. Gomes, J. Lubian, L. C. Chamon, and E. Crema, Nucl. Phys. A **821**, 51 (2009).
[33] C. Y. Wong, Phys. Rev. Lett. **31**, 766 (1973).
[34] J. M. B. Shorto, P. R. S. Gomes, J. Lubian, L. F. Canto, and P. Lotti, Phys. Rev. C **81**, 044601 (2010).
[35] P. R. S. Gomes, L. F. Canto, L. Lubian, P. Lotti, L. C. Chamon, E. Crema, and J. M. B. Shorto, Nucl. Phys. A **834**, 151c (2010).

[36] J. Fernández-Niello, C. H. Dasso, and S. Landowne, Comput. Phys. Commun. **54**, 409 (1989).
[37] S. Raman, C. W. Nestor Jr., and P. Tikkanen, At. Data Nucl. Data Tables **78**, 1 (2001).
[38] T. Kibédi and R. H. Spear, At. Data Nucl. Data Tables **80**, 35 (2002).
[39] D. L. Hill and J. A. Wheeler, Phys. Rev. **89**, 1102 (1953).
[40] V. I. Zagrebaev and V. V. Samarin, Phys. At. Nucl. **67**, 1462 (2004).
[41] W. Henning, F. L. H. Wolfs, J. P. Schiffer, and K. E. Rehm, Phys. Rev. Lett. **58**, 318 (1987).
[42] P. R. S. Gomes, A. M. M. Maciel, R. M. Anjos, S. B. Moraes, R. Liguori Neto, R. Cabezas, C. Muri, G. M. Santos, and J. F. Liang, J. Phys. G **23**, 1315 (1997).